STAR Protocols

CellPress
OPEN ACCESS

Protocol

Functional Multiple-Spine Calcium Imaging from Brain Slices

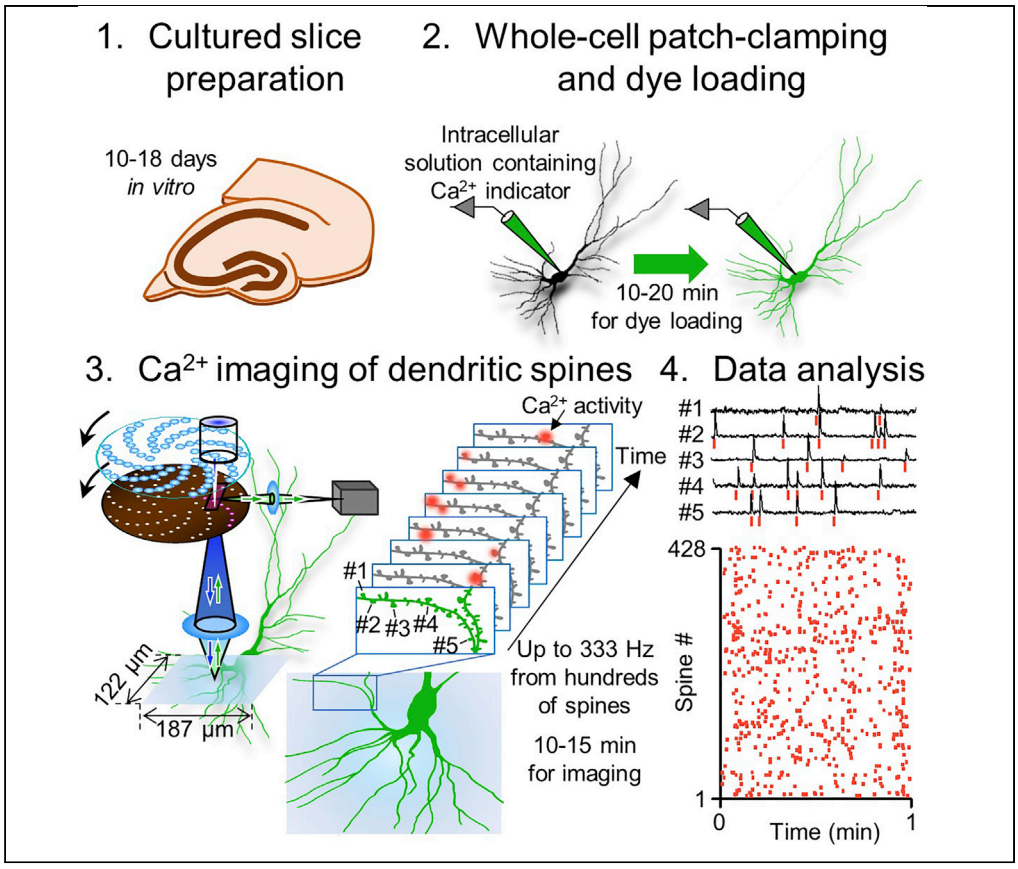

Most excitatory inputs arrive at dendritic spines in a postsynaptic neuron. To understand dendritic information processing, it is critical to scrutinize the spatiotemporal dynamics of synaptic inputs along dendrites. This protocol combines spinning-disk confocal imaging with whole-cell patch-clamp recording to perform wide-field, high-speed optical recording of synaptic inputs in a neuron loaded with a calcium indicator in *ex vivo* cultured networks. Our protocol enables simultaneous detection of synaptic inputs as calcium signals from hundreds of spines in multiple dendritic branches.

Tomoe Ishikawa,
Chiaki Kobayashi,
Naoya Takahashi,
Yuji Ikegaya

tomoe.y.ishikawa@gmail.com

HIGHLIGHTS

Simultaneous calcium imaging of synaptic activity from hundreds of spines in vitro

Whole-cell voltage clamping for dye loading and signal improvement

Photobleaching-free and photodamage-free imaging of synaptic activity by spinning-disk confocal system

A modified median filter for effective denoising of optical signals

Ishikawa et al., STAR Protocols *1*, 100121
December 18, 2020
https://doi.org/10.1016/j.xpro.2020.100121

STAR Protocols

CellPress
OPEN ACCESS

Protocol

Functional Multiple-Spine Calcium Imaging from Brain Slices

Tomoe Ishikawa,[1,3,4,*] Chiaki Kobayashi,[1] Naoya Takahashi,[1] and Yuji Ikegaya[1,2]

[1]Graduate School of Pharmaceutical Sciences, The University of Tokyo, Tokyo 113-0033, Japan

[2]Center for Information and Neural Networks, National Institute of Information and Communications Technology, Suita City, Osaka, 565-0871, Japan

[3]Technical Contact

[4]Lead Contact

*Correspondence: tomoe.y.ishikawa@gmail.com
https://doi.org/10.1016/j.xpro.2020.100121

SUMMARY

Most excitatory inputs arrive at dendritic spines in a postsynaptic neuron. To understand dendritic information processing, it is critical to scrutinize the spatiotemporal dynamics of synaptic inputs along dendrites. This protocol combines spinning-disk confocal imaging with whole-cell patch-clamp recording to perform wide-field, high-speed optical recording of synaptic inputs in a neuron loaded with a calcium indicator in *ex vivo* cultured networks. Our protocol enables simultaneous detection of synaptic inputs as calcium signals from hundreds of spines in multiple dendritic branches.

For complete details on the use and execution of this protocol, please refer to Takahashi et al. (2012, 2016), Kobayashi et al. (2019), and Ishikawa and Ikegaya (2020).

BEFORE YOU BEGIN

Nonlinear dendritic computations depend largely on the spatiotemporal patterns of excitatory synaptic inputs (Losonczy et al., 2008; Branco et al., 2010; Poirazi et al., 2003). However, due to technical limitations, how synaptic inputs are organized in space and time along dendrites is still poorly understood. A unique approach to investigate the spatiotemporal patterns of synaptic input is spine calcium imaging using calcium ion-sensitive fluorophores, which captures synaptic inputs as calcium transients at individual spines (Müller and Connor, 1991; Guthrie et al., 1991). The conventional technique for spine calcium imaging was based on epifluorescence microscopy and was subject to severe photobleaching and photodamage, and the signal-to-noise (SN) ratios were insufficient for high-speed and large-scale monitoring. Two-photon microscopy was used to overcome these problems. Since Yuste and Denk (Yuste and Denk, 1995) first succeeded in detecting individual activity simultaneously in a few spines, techniques for functional multiple-spine calcium imaging (fMsCI) have been adapted to study the spatiotemporal structures of inputs (Varga et al., 2011; Chen et al., 2012); however, it remains challenging to monitor the activity of a large number of spines, especially in intact brain tissues. This limitation is mainly due to the opacity of brain tissues, which causes undesired absorption and scattering of photons, reducing the SN ratio; if the power of excitation light is increased to improve the SN ratio, then photodamage and photobleaching become serious concerns. Therefore, it is still difficult to achieve large-scale fMsCI from multiple dendritic branches at high frame rates.

To reduce light scattering, we use organotypically cultured *ex vivo* neuronal networks. In *ex vivo* preparations, isolated brain slices spontaneously recover without external afferents during cultivation. The self-organized neuronal networks in these slices may involve aberrant circuits to some

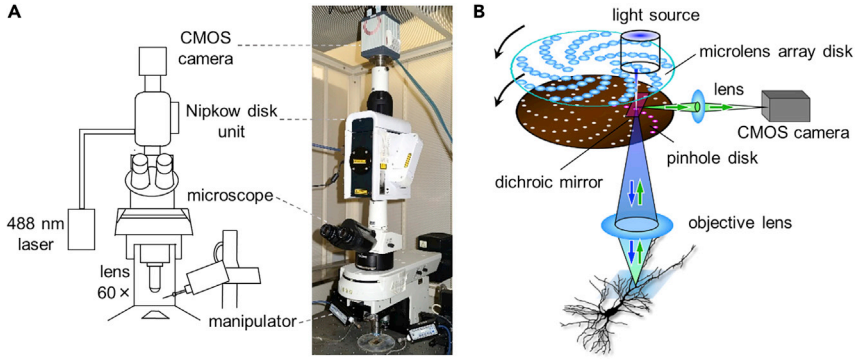

Figure 1. Spinning-Disk Confocal Microscopy for fMsCI

(A) Diagram of an experimental setup. The CMOS camera and Nipkow-type confocal unit are mounted on an upright microscope equipped with a 60× objective lens and a 488-nm laser box.

(B) Schematic illustration of the optical system. A 488-nm laser passes through a microlens-array disk and a rotating pinhole-array disk and splits into multiple beams before reaching the specimen. The emitted fluorescence passes through the same pinhole-array disk and is collected by a CMOS camera.

extent (Sakaguchi et al., 1994), but as a whole, they preserve *in vivo*-like neuronal connectivity patterns and exhibit spontaneous neuronal activity that resembles *in vivo* neuronal activity (Takahashi et al., 2010; Okamoto et al., 2014). More importantly, the opacity of the brain parenchyma is reduced during cultivation. This optical transparency is advantageous for fMsCI: the excitation laser intensity can be decreased to achieve practical SN ratios, and photobleaching and phototoxicity are avoided.

To monitor the calcium activity of hundreds of spines from multiple dendritic trees of a neuron in an *ex vivo* network, we established a new optical recording technique for fMsCI (Takahashi et al., 2012; Takahashi et al., 2016; Ishikawa and Ikegaya, 2020). In our protocol, we combined a Nipkow-type spinning-disk confocal unit with a CMOS camera (Figure 1A). A Nipkow-disk confocal microscope uses multisite focal illumination and detects photons nearly simultaneously from the entire field of view of the microscope, while conventional raster-scanning confocal microscopes can scan only a single spot in the field at a time. A rotating disk used in a Nipkow-type microscope has tens of thousands of pinholes, through which the excitation laser is split into an array of rays and covers the entire field of view (Figure 1B). The emitted light is detected by a CMOS camera, which has high quantum efficiency and low noise (Long et al., 2012). A high-end Nipkow-type microscope achieves a scanning speed of up to 2,000 frames per second (Takahashi et al., 2010). Nipkow-disk units also reduce photobleaching and phototoxicity, probably because the laser intensity of each single ray in a laser array is low. In general, the photobleaching rates increase as a supralinear function of light intensity (Takahashi et al., 2011). In Nipkow-disk confocal microscopy, fluorophores are excited many times by weak lasers, and the emitted photons are collected and averaged online by a CMOS sensor. Therefore, functional multiple-spine calcium imaging (fMsCI) using Nipkow-disk microscopy attains high SN ratios and low photobleaching rates and thereby allows continuous long-term calcium imaging at high frame rates. With this method, we succeeded in imaging an average of approximately 244 dendritic spines per video (n = 32 videos, up to 428 spines) at 100–333 Hz.

Prepare Equipment for Calcium Imaging

Timing: 3 h; to be completed at least a day before the experiment

1. Spinning-disk confocal microscope setup (Figure 1).
   a. Mount a spinning-disk confocal unit on an upright microscope using a C-mount connecting adaptor.

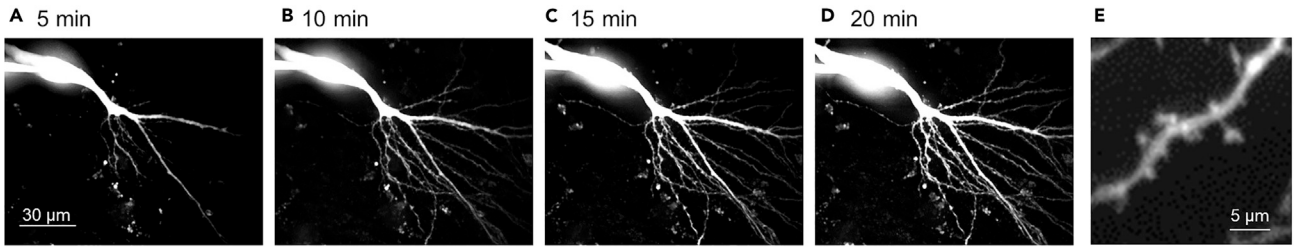

Figure 2. Time-Lapse Confocal Images of Dendritic Branches in the Whole-Cell Configuration Using a Patch-Clamp Pipette Loaded with Fluo-4

(A–D) Fluo-4 was gradually loaded into dendrites as indicated.

(E) An enlarged view of a dendritic branch and spines at 20 min using a 60× objective lens and a 2× optical magnifier turret.

b. Mount a water-cooled Hamamatsu complementary metal-oxide-semiconductor (CMOS) camera on the confocal unit. We also used an electron multiplying charge coupled device (EM-CCD) camera (Andor) in our previous studies (Takahashi et al., 2016; Takahashi et al., 2012). Other compatible CMOS or EM-CCD cameras with wide imaging fields and high spatial resolutions (more than 500 × 500 pixels) can also be used.

c. **Optional:** Intercalate an optical magnifier turret between the microscope and the confocal unit. We routinely apply 2× optical magnification for imaging (Figure 2).

d. Deliver a 488-nm laser into the confocal unit. A Nipkow disk split the laser beam into multiple lasers. The microlens array on the Nipkow disk is designed to minimize light loss by focusing each laser beam on the corresponding pinhole.

e. Use a 488-nm laser to excite the fluorophores, and the fluorescent signals are captured through a 507-nm long-pass emission filter.

f. Acquire images at 100–333 frames per second (Hz).

⚠ CRITICAL: The spinning-disk system is essential for this protocol. In our lab, we used a Yokogawa spinning-disk unit (CSU-X1) and a Nikon upright microscope. The CSU is equipped with a laser system and two coaxially aligned disks (Figure 1B), which improves light efficiency to take bright images.

⚠ CRITICAL: One of the advantages of Nipkow-type spinning-disk confocal microscopy is that it enables online experimental manipulations owing to the fast scanning rates (up to 2,000 Hz). Another important advantage is its slow photobleaching (and thus low phototoxicity). Increasing laser power nonlinearly accelerates photobleaching (Takahashi et al., 2011). As the Nipkow disk splits the laser into multiple beams, the intensity of each split beam is considerably low (~1–5 μW), resulting in negligible photobleaching during the course of an experiment. Conventional epifluorescence microscopy is not adequate for our protocols because of its fast photobleaching.

⚠ CRITICAL: Use an objective with a high numerical aperture. We routinely use a 60× objective lens which has 1.0 NA. We also use a 40× objective lens which has 0.8 NA in our previous research. An objective with a long working distance is desirable to prevent interference with patch pipettes. The Yokogawa CSU-X1 confocal unit can obtain images that are approximately twice as bright as those captured by the older versions, CSU10 and CSU22.

2. Setup patch-clamp instrument.
Refer to Materials and Equipment.

Reagent Preparation

Timing: 3 h

3. Prepare Hanks' balanced salt solution (HBSS).

Refer to Materials and Equipment for buffer recipe.

4. Prepare Gey's balanced salt solution (GBSS).

Refer to Materials and Equipment for buffer recipe.

5. Prepare intracellular solution (for EPSC or IPSC recording).

Refer to Materials and Equipment for buffer recipe.

6. Prepare Fluo-4 or Fluo-5F stock solutions.

Dissolve the entire vial of Fluo-4 (or Fluo-5F) pentapotassium salt with intracellular solution to 1 mM and aliquot 20 μL into a 0.6-mL tube. The solution can be stored for several weeks at −20°C.

Preparation of Cultured Brain Slices

Timing: 90 min, start 10–18 days before the imaging

Prepare organotypically cultured brain slices. We usually use 6 to 8-day-old rats for cultured hippocampal slices. Further details can be found in references (Bischofberger et al., 2006; De Simoni and Yu, 2006; Koyama et al., 2007).

7. Anesthetize rats with hypothermia on ice or isoflurane in an anesthetizing chamber until the loss of nociceptive reflex.
8. Decapitate rats, remove the brains, and place brains into ice-cold oxygenated GBSS.
9. Prepare 300-μm-thick horizontal whole-brain slices with a vibratome (speed: 20–27 mm/min) in ice-cold oxygenated GBSS. Trim entorhinal-hippocampal region in ice-cold oxygenated GBSS using a surgical microknife.
10. Place two to three slices on an Omnipore membrane filter in a 35-mm dish with 1 mL of culture medium (De Simoni and Yu, 2006).
11. Place the dishes in a cell culture incubator with 5% CO_2 at 37°C.
12. Change the culture medium every 3–4 days.

Note: Slices cultured for 10–18 days *in vitro* are suitable for this protocol.

KEY RESOURCES TABLE

REAGENT or RESOURCE	SOURCE	IDENTIFIER
Chemicals, Peptides, and Recombinant Proteins		
NaCl	Nacalai Tesque	cat. no. 31320-05
KCl	Nacalai Tesque	cat. no. 28513-85
$NaHCO_3$	Nacalai Tesque	cat. no. 31213-15
$NaH_2PO_4 \cdot 2H_2O$	Nacalai Tesque	cat. no. 31718-15
$Na_2HPO_4 \cdot 12H_2O$	Nacalai Tesque	cat. no. 31723-35
KH_2PO_4	Nacalai Tesque	cat. no. 28721-55

(*Continued on next page*)

Continued

REAGENT or RESOURCE	SOURCE	IDENTIFIER
$CaCl_2 \cdot 2H_2O$	Nacalai Tesque	cat. no. 06730-15
$MgCl_2 \cdot 7H_2O$	Nacalai Tesque	cat. no. 20908-65
$MgSO_4 \cdot 7H_2O$	Nacalai Tesque	cat. no. 21002-85
D-glucose	Nacalai Tesque	cat. no. 16806-25
$CsMeSO_4$	Sigma-Aldrich	cat. no. C1426-5G
CsCl	Nacalai Tesque	cat. no. 07806-92
HEPES	Sigma-Aldrich	cat. no. H4034-500G
Mg-ATP	Sigma-Aldrich	cat. no. A9187-500MG
Na_2-GTP	Sigma-Aldrich	cat. no. G8877-25MG
Na-phosphocreatine	Sigma-Aldrich	cat. no. P7936-5G
Trolox	Sigma-Aldrich	cat. no. 238813-1G
Fluo-4 pentapotassium salt	Thermo Fisher Scientific	F14200
Fluo-5F pentapotassium salt	Thermo Fisher Scientific	F14221
Heat-inactivated horse serum	Thermo Fisher Scientific	cat. no. 26050-088
Minimal essential medium (MEM)	Nacalai Tesque	cat. no. 21442-25
Penicillin/streptomycin	Sigma-Aldrich	cat. no. P4333
Carbogen (a mixture of 95% oxygen and 5% carbon dioxide)	N/A	N/A
Experimental Models: Organisms/Strains		
Rat: aged 6–8 days (neither the strain nor the sex of the animals is important for this protocol)	SLC	N/A
Software and Algorithms		
High Speed Recording software ver. 2.3 (HSR)	Hamamatsu Photonics	N/A
pCLAMP 10.3 software	Molecular Devices	N/A
MATLAB	MathWorks	N/A
Fiji/ImageJ	Schindelin et al., 2012	N/A
Other		
Scissors, forceps, and spatula	N/A	N/A
Vibrating slicer	Dosaka	cat. no. DTK-1500
Membrane filter	Millipore	Omnipore JHWP02500, diameter: 25 mm, 0.45-μm pores
O-shaped plastic plate, termed a "doughnut" plate	Hazai-Ya (Koyama et al., 2007)	N/A
Scalpel	FEATHER	FEATHER DISPOSABLE SCALPEL 20×, No.14
Upright microscope	Nikon	cat. no. FN-1
Water-immersion objective lens (magnification: 60×)	Nikon	NIR Apo 60XW
Optical magnifier turret	Nikon	1×, 1.5×, 2×
Microscope isolation system with an XY mover	Narishige	cat. no. ITS-FN1
Nipkow-type spinning-disk confocal unit	Yokogawa	cat. no. CSU-X1
CMOS camera	Hamamatsu Photonics	ORCA-Flash4.0 V2, cat. no. C11440-22CU
Laser diode 488 nm	TAC	LDSYS-488/561

(*Continued on next page*)

Continued

REAGENT or RESOURCE	SOURCE	IDENTIFIER
Inline solution heater	Warner Instruments	cat. no. SH-27B
Temperature controller	Warner Instruments	cat. no. TC-344B
U-shaped platinum anchor to weigh down slices in the recording chamber	N/A	N/A
Electromotive micromanipulator	Narishige	cat. no. EMM-3NV
Patch-clamp amplifier	Molecular Devices	cat. no. MultiClamp 700B or Axopatch 200B
Horizontal electrode puller	Sutter Instruments	P-1000 horizontal puller
Microforge	Narishige	cat. no.MF-830
Thick-walled borosilicate glass tubing (outer diameter: 1.5 mm, inner diameter: 0.84 mm)	World Precision Instruments	cat. no. 1B150F-4
Patch pipette fillers with a solution filter (diameter: 4 mm, 0.45-μm pores)	Millipore	Millex-LH
Syringe pressurizer (10 mL)	Terumo	N/A
C-mount connecting adaptor	N/A	N/A
Electronic stimulator	Nihon Kohden	cat. no. SEN-3301

MATERIALS AND EQUIPMENT

Patch-Clamp Instrument Setup

Useful methods for the assembly of a functional patch-clamp setup can be found in the Molecular Devices Axon Guide. No special setups for spine imaging are required.

Pipette Puller

We use a dual-carriage (horizontal) puller. In general, the puller has several parameters, including the number of pulling cycles, pulling strength, heating duration and temperature, and cooling gas flow. The number of pulling cycles should be between three and five. The ideal shape of pipettes for culture slice whole-cell patch-clamping is a short taper and low resistance (4–6 MΩ). Low pulling strength is better to reduce variations in tip shapes. Further details can be found in a pipette cookbook from Sutter Instrument [https://www.sutter.com/PDFs/pipette_cookbook.pdf].

Optional: Fire-polish the tip of pipettes to obtain the appropriate diameter and resistance.

Artificial Cerebrospinal Fluid (aCSF)

Reagent	Final Concentration	Amount
NaCl	126.5 mM	7.39 g
KCl	3.5 mM	0.26 g
$CaCl_2 \cdot 2H_2O$	2.4 mM	0.35 g
$MgCl_2 \cdot 7H_2O$	1.3 mM	0.16 g
$NaHCO_3$	26 mM	2.18 g
$NaH_2PO_4 \cdot 2H_2O$	1.24 mM	0.19 g
D-glucose	10 mM	1.80 g
Trolox	0.4 mM	0.10 g
ddH_2O	n/a	~1 L
Total	n/a	1 L

⚠ CRITICAL: aCSF should be prepared on the day of the experiment and saturated with carbogen (95% O_2/5% CO_2) for at least 10 min.

Gey's Balanced Salt Solution (GBSS)

Reagent	Final Concentration	Amount
NaCl	120 mM	7.01 g
KCl	5 mM	0.37 g
$CaCl_2 \cdot 2H_2O$	1.5 mM	0.22 g
$MgCl_2 \cdot 6H_2O$	1 mM	0.21 g
$MgSO_4 \cdot 7H_2O$	0.57 mM	0.14 g
$NaHCO_3$	27 mM	2.27 g
$Na_2HPO_4 \cdot 12H_2O$	0.8 mM	0.29 g
KH_2PO_4	0.22 mM	0.03 g
D-glucose	36 mM	6.50 g
ddH_2O	n/a	~1 L
Total	n/a	1 L

⚠ CRITICAL: The solution must be filter sterilized before use. Fleshly prepare the solution just before each experiment.

Hanks' Balanced Salt Solution (HBSS)

Reagent	Final Concentration	Amount
NaCl	137 mM	8.01 g
KCl	5.4 mM	0.40 g
$CaCl_2 \cdot 2H_2O$	1.3 mM	0.19 g
$MgCl_2 \cdot 6H_2O$	0.5 mM	0.10 g
$MgSO_4 \cdot 7H_2O$	0.6 mM	0.07 g
$NaHCO_3$	4.2 mM	0.35 g
$Na_2HPO_4 \cdot 12H_2O$	0.3 mM	0.11 g
KH_2PO_4	0.4 mM	0.05 g
D-glucose	5.6 mM	1.01 g
ddH_2O	n/a	~1 L
Total	n/a	1 L

⚠ CRITICAL: The solution must be filter sterilized before use. Freshly prepare the solution just before each experiment.

Intracellular Solution (EPSC Recording)

Reagent	Final Concentration	Amount
$CsMeSO_4$	47.7 mM	1.09 g
CsCl	92.3 mM	1.55 g
HEPES	10 mM	0.24 g
Na-phosphocreatine	10 mM	0.26 g
Mg-ATP	4 mM	0.20 g
Na_2-GTP	0.3 mM	0.016 g
ddH_2O	n/a	~100 mL
Total	n/a	100 mL

⚠ CRITICAL: This intracellular solution is used for EPSC recording at −30 mV. Adjust the pH of the solution with CsOH to 7.2–7.3 and check osmolarity of the solution. For patch-clamping, 280–290 mOsm/L is good. The solution can be stored for several weeks at −20°C. Keep the solution on ice throughout the experiment.

Intracellular Solution (IPSC Recording)

Reagent	Final Concentration	Amount
$CsMeSO_4$	130 mM	2.96 g
CsCl	10 mM	0.17 g
HEPES	10 mM	0.24 g
Na-phosphocreatine	10 mM	0.26 g
Mg-ATP	4 mM	0.20 g
Na_2-GTP	0.3 mM	0.016 g
ddH_2O	n/a	~100 mL
Total	n/a	100 mL

⚠ CRITICAL: This intracellular solution is used for IPSC recording at −30 mV. Adjust the pH of the solution with CsOH to 7.2–7.3 and check osmolarity of the solution. For patch-clamping, 280–290 mOsm/L is good. The solution can be stored for several weeks at −20°C. Keep the solution on ice throughout the experiment.

Culture Medium

Reagent	Final Concentration	Amount
MEM	n/a	50 mL
HBSS	n/a	25 mL
heat-inactivated horse serum	25%	25 mL
antibiotics (Penicillin-Streptomycin)	5 unit/mL penicillin and 5.0 μg/mL streptomycin	50 μL
Total	n/a	100 mL

⚠ CRITICAL: Freshly prepare the solution just before each experiment.

STEP-BY-STEP METHOD DETAILS

Reagent and Pipette Preparation on the Day of the Experiment

Timing: 30–60 min

1. Prepare artificial cerebrospinal fluid (aCSF).

Refer to Materials and Equipment for buffer recipe.

2. Prepare patch-clamp pipettes.

Prepare standard pipettes (4–6 MΩ) for somatic recordings. There is no need to prepare pipettes with designated shapes for spine imaging. Refer to Materials and Equipment for more information.

3. Dissolve a 20 μl aliquot of 1 mM stock solution of Fluo-4 (or Fluo-5F) pentapotassium salt with intracellular solution to a final concentration of 200 μM

⚠ CRITICAL: Keep the solution on ice throughout the experiment.

Somatic Recording and Dye Loading

Timing: 30–60 min

4. Cut the membrane around a slice using a surgical microknife and transfer the slice to a recording chamber that is perfused with aCSF warmed to 32–34°C.

⚠ CRITICAL: Perfuse the slice with 200 μM Trolox, which is an antioxidant, in aCSF to reduce phototoxicity and photobleaching.

⚠ CRITICAL: The speed of aCSF perfusion should be kept at 2–4 mL/min.

⚠ CRITICAL: For good recordings, use slices within 4 h after transferring them to the chamber.

5. Place a platinum anchor on the slice membrane to keep the slice from being dislodged by the perfusion solution.

⚠ CRITICAL: Trim the membrane to leave enough room for the platinum anchor.

6. Stabilize the slice in the recording chamber for 15 min to reduce the movement of the slice during recording.
7. Search and focus on a healthy neuron with a 60× objective lens. If necessary, use a differential interference contrast or gradient contrast video microscope to facilitate patch-clamping.
8. To load the dendrites with a calcium indicator, perform whole-cell recording from the soma with the intracellular solution containing 200 μM Fluo-4 (or Fluo-5F, cf. Expected Outcomes and Limitations). Use a glass pipette with a resistance of 4–6 MΩ to obtain an access resistance of ~20 MΩ. Carefully approach the selected soma with a positive pressure of 50–100 kN/m^2. Once the pipette tip has been positioned, release the pipette pressure and apply gentle suction (~20 kN/m^2). The patch configuration can be assessed by applying repetitive 10-mV test pulses using a patch-clamp amplifier.

⚠ CRITICAL: Access resistance should be kept below 20 MΩ to attain good voltage-clamp performance in the following steps.

9. After constructing the whole-cell configuration, wait until the dendrites are sufficiently labeled with the calcium indicator. For pyramidal cells in the neocortex or hippocampus, this step takes ~10 min.

⚠ CRITICAL: This period is a tradeoff. A longer time achieves a greater intensity of fluorescence at the dendritic branches (Figure 2) but makes cells more sensitive to phototoxicity.

⚠ CRITICAL: This period depends on the quality of the whole-cell configuration. Higher access resistance requires a longer time to load the dendrites with the dye.

⚠ CRITICAL: To avoid phototoxicity and photobleaching, do not expose the cell to light.

10. Adjust the parameters of image acquisition for optimal results. We find that the following settings work best: frame rates, 100–333 Hz; and spinning-disk rotation speeds, 5,000–10,000 rotations per minute (rpm) (Figures 3 and 4).

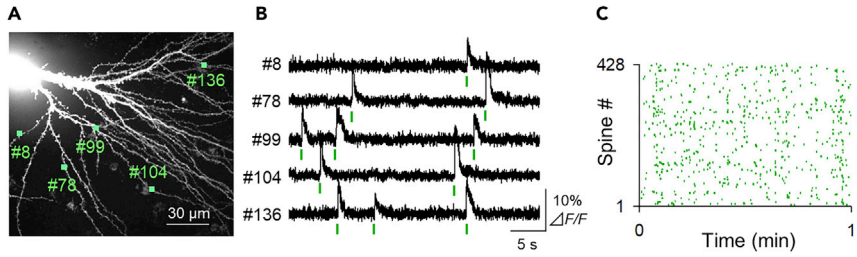

Figure 3. fMsCI Data

(A) A confocal snapshot of dendritic trees of a Fluo-4-loaded CA3 pyramidal neuron in a cultured hippocampal slice.

(B) Representative raw traces of the calcium activity of five spines recorded at a frame rate of 333 Hz. The spine numbers correspond to those in panel A.

(C) A representative raster plot of spine activity. The activity of 428 spines was simultaneously recorded for 1 min.

⚠ CRITICAL: The rest of the procedure should be performed as rapidly as possible to avoid phototoxicity and photobleaching. If the total duration of laser exposure exceeds 10 min, undesirable side effects may occur in the cells. Damage may be observed, such as the beading of dendritic varicosities and an extremely high dendritic fluorescence regardless of holding potential.

Calcium Imaging of Dendritic Spines

Timing: 10–15 min

11. Switch to the voltage-clamp mode for current recording, and set the holding voltage at −30 mV (Figure 5).

12. Find an appropriate region of the dendritic field of the patched neuron and place the region in the center of the field of view. Troubleshooting 1.

⚠ CRITICAL: To minimize the space-clamp effect, only spines located within 200 μm of the soma should be imaged.

⚠ CRITICAL: Try to minimize laser power to prevent photodamage.

13. Adjust the laser intensities for optimal results. We find that less than 1 mW is suitable for this protocol.

⚠ CRITICAL: Low laser power is recommended to prevent photodamage; first, start with lower power, and then adjust to obtain a sufficient SN ratio.

14. Start image acquisition for a time period for the purpose of the experiment. Troubleshooting 2, 3, and 4.

⚠ CRITICAL: In some cases, the images may contain wave-like periodic noise (*i.e.*, interference fringes due to differential interaction between the rotation speed of the Nipkow disk and the camera scanning rate (Takahashi et al., 2011)). To reduce the interference, adjust the rotational speed of the disk or the video rate.

⚠ CRITICAL: If necessary, record EPSCs or IPSCs simultaneously with spine activity (Figure 6). We use a transistor–transistor logic (TTL) trigger with a stimulator to synchronize imaging and electrophysiology recording.

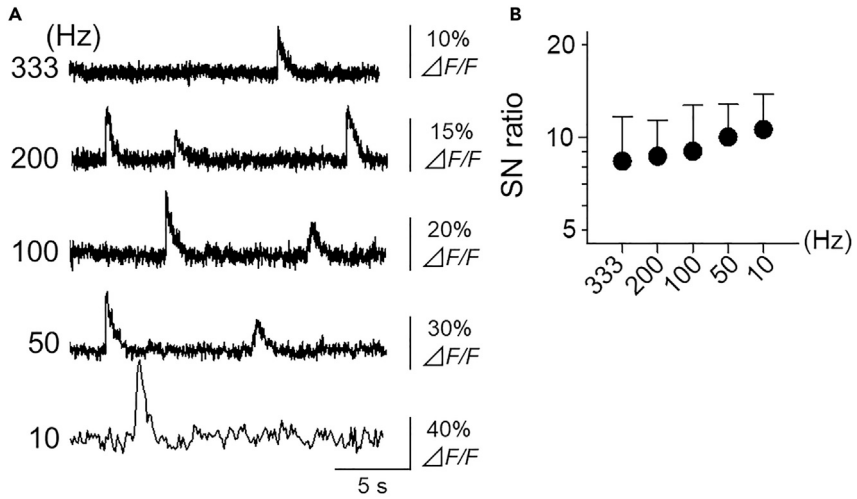

Figure 4. Effects of Video Frame Rates on SN Ratios of Spine Calcium Activity

(A) Representative raw traces of calcium activity in a Fluo-4-loaded spine recorded at frame rates of 333, 200, 100, 50, and 10 Hz.

(B) Means ± SDs of SN ratios of 20 spines at five different frame rates. $P = 0.15$, $F_{4,95} = 1.78$, one-way ANOVA.

15. Acquire a z-stack of images of the dendritic branches for post hoc three-dimensional reconstruction of the recorded spines (frame rate: 1 frame/s).

⚠ CRITICAL: The framerate is important for a clear z-stack image; it should be less than 10 frames/s.

Pause Point: The following data analysis steps can be performed at a later date.

Analysis of Spine Calcium Signals

Timing: hours to days

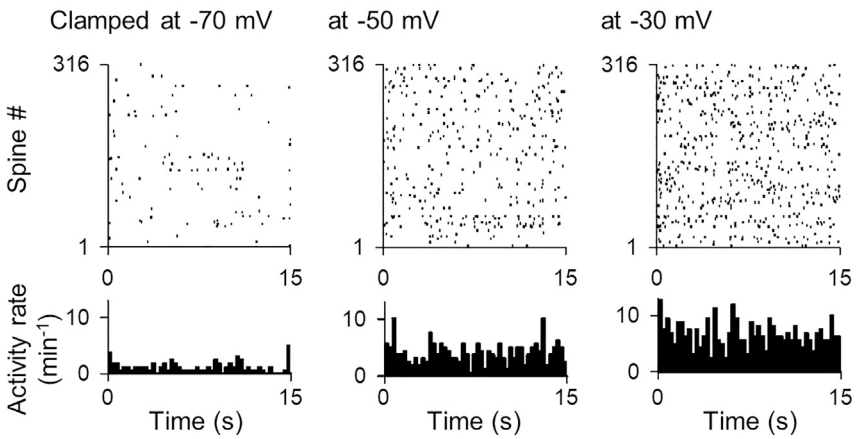

Figure 5. Effects of Clamped Voltages on Recorded Spine Calcium Activity Rates

The membrane potential of a CA3 pyramidal cell was clamped at −70 mV, −50 mV, and −30 mV. More spine calcium activity was detected at higher voltages, suggesting that spine activity is mediated by voltage-sensitive calcium influxes.

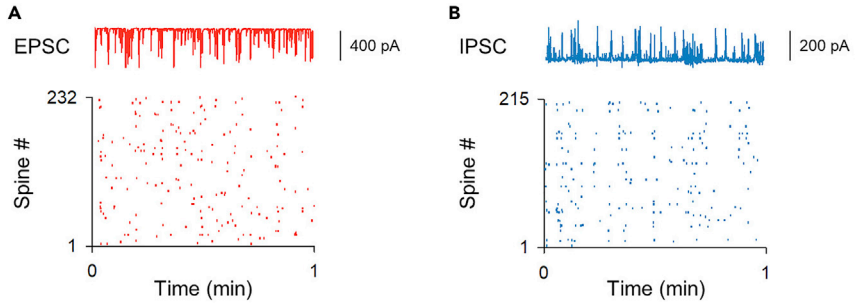

Figure 6. Recording Somatic EPSCs or IPSCs (Clamping at −30 mV Respectively) Simultaneously with Spine Calcium Activity

(A) A representative raw trace of somatic EPSCs and a raster plot of spine activity.

(B) The same as (A) but for IPSCs.

16. Determine the regions of interest (ROIs) that encompass the recorded spines. We manually draw ROIs based on the coordinate of the center of a given spine and the radius of the spine (Figure 7). Individual ROIs covered 1.38 ± 0.67 μm^2 (ROIs on 7,750 spines from 32 cells). Troubleshooting 5.

⚠ CRITICAL: ROIs should match the spine contours; otherwise, the fluorescent signal may be contaminated by that of neighboring spines. We routinely analyze data using the freely available Fiji/ImageJ software and the MATLAB.

17. Average the fluorescence intensities of all pixels within each ROI for each frame and generate a time series of the mean fluorescence for individual spines.
18. Apply the modified Okada filter to the time series of the mean fluorescence (generated in step 17) according to the formula in the box of Figure 8A, which reduces shot noise under low SN ratio conditions.

⚠ CRITICAL: If noise remains, reapply the modified Okada filter (Figure 9).

19. Extract signals from calcium fluctuations.

⚠ CRITICAL: The timing of spine activity is manually or automatically determined based on the onsets of calcium transients (Sasaki et al., 2008).

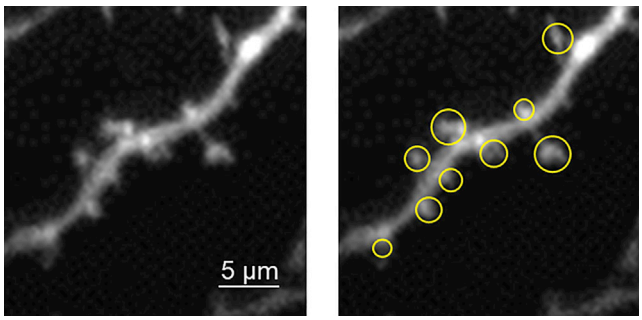

Figure 7. Representative ROIs on Dendritic Spines

Manually drawn ROIs are determined by the coordinate of the center of a given spine and the radius of the spine (right).

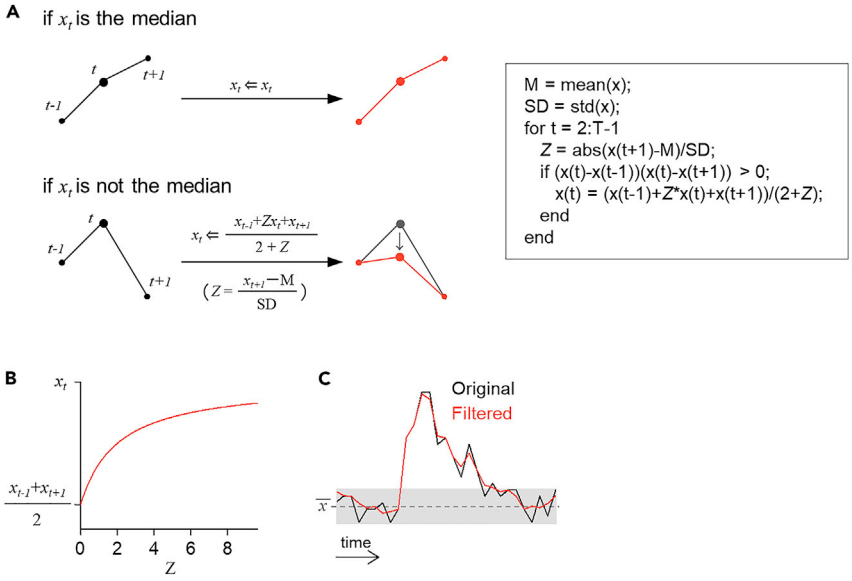

Figure 8. Modified Okada Filter

(A) Schematic illustration of data processing with a modified Okada filter (left). The fluorescence intensity, x_t, at the focused time, t, is compared with the preceding and following values, x_{t-1}, and x_{t+1}, respectively. If x_t is the median among x_{t-1}, x_t, and x_{t+1}, that is, if $(x_t - x_{t-1})(x_t - x_{t+1}) \leq 0$, then x_t is not changed (top). If x_t is not the median, that is, if $(x_t - x_{t-1})(x_t - x_{t+1}) > 0$, then x_t is replaced with $(x_{t-1} + Zx_t + x_{t+1})/(2 + Z)$ (bottom). The coefficient Z is defined as $(x_{t+1} - M)/SD$, where the mean M and the standard deviation SD are calculated from the entire time series $\{x_t\}$.

(B) The substituted value $(x_{t-1} + Zx_t + x_{t+1})/(2 + Z)$ is plotted as a function of Z. When Z is 0, x_t is substituted with the mean of x_{t-1} and x_{t+1}, i.e., $(x_{t-1} + x_{t+1})/2$. When Z takes higher values, $(x_{t-1} + Zx_t + x_{t+1})/(2 + Z)$ becomes closer to x_t.

(C) The original trace (black) was processed by the modified Okada filter (red). The gray dashed line and area indicate the M and SD values of the original trace.

EXPECTED OUTCOMES

In our experimental protocol, a neuron is whole-cell patch clamped using a borosilicate glass pipette through which fluorescent calcium indicators are intracellularly injected. Within 20 min after the whole-cell patch-clamp is established, individual spines are loaded with the indicators (Figure 2). Our imaging apparatus consists of a CSU-X1 Nipkow-disk confocal microscope, an ORCA-Flash4.0 CMOS camera, and a 60× water-immersion objective lens, covering a visual field of 187 μm × 122 μm. Using this equipment, we recorded calcium activity in up to 428 spines from a single hippocampal pyramidal cell (Figure 3). More spine calcium events are detected when the membrane potential is voltage clamped at −30 mV than at −50 mV or −70 mV (Figure 5). In the soma, the frequency of excitatory postsynaptic currents *per se* is not affected by the clamped voltage (Kobayashi et al., 2019). These results indicate that transient calcium increases are mediated by calcium influx through voltage-sensitive channels, such as *N*-methyl-D-aspartate (NMDA) receptors. Consistent with this idea, spine calcium activity is abolished by bath application of D-(-)-2-amino-5-phosphonopentanoic acid (D-AP5), an NMDA receptor antagonist, and is facilitated by the application of D-serine, an NMDA receptor sensitizer (Figure 10). These chemicals do not affect the activity rates recorded from the somata (Figure 10). Thus, the modulation of spine activity is attributable to changes in the open probability of NMDA receptor channels in postsynaptic spines but not in the presynaptic activity level. A total of 20.7% of the calcium activity in dendritic spines (442/2136 Ca^{2+} transients from four cells) was accompanied with calcium activity in dendritic shafts near the spines within ± 30 ms of the activity in the dendritic spines. A total of 7.0% (149/2136 Ca^{2+} transients) of the spine calcium activity was preceded by the calcium activity in the dendritic shaft near the spine. This result implies that less than 7.0% of the recorded Ca^{2+} activity in spines resulted from localized dendritic spikes and that most of the Ca^{2+} activity resulted from synaptic input. Attention must be paid to these data because

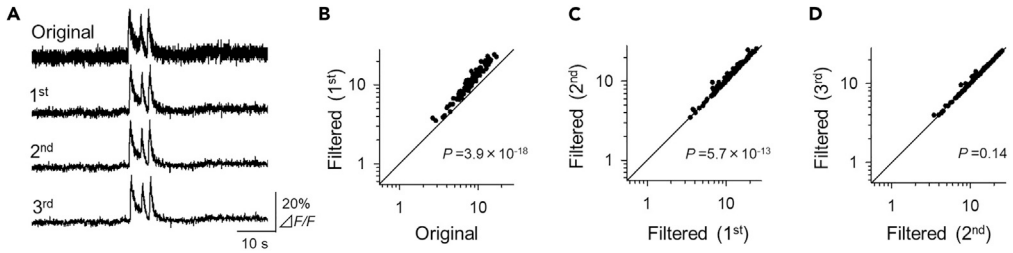

Figure 9. Effect of Repetitive Noise Reductions Using the Modified Okada Filter on the SN Ratios of Spine Calcium Activity

(A) A raw original trace of calcium activity recorded from a Fluo-4-loaded spine at a video frame rate of 2,000 Hz (top) was repeatedly filtered using the modified Okada filter.

(B–D) The SN ratios of 100 original traces (B) are compared before (C) and after (D) the application of the modified Okada filter. The SN ratio was improved by the first two applications of the filter. *P* was determined using the Wilcoxon signed-rank test for 100 spines from ten cells.

our observation was conducted in the voltage-clamp configuration that could reduce dendritic summation and dendritic spiking. To avoid a space-clamp problem, we monitored only spines located within 200 μm of the cell bodies.

Higher video frame rates provide higher temporal resolution in recordings of spine calcium activity, but there is a tradeoff between the frame rate and the SN ratio: higher frame rates result in lower SN ratios in calcium fluorescence (Figure 4). In our systems, 2,000 Hz is the theoretical maximum frame rate for full-screen imaging. We have confirmed that we can record Ca^{2+} signals with high SN ratio at 333 Hz. Less than 50 Hz is not enough to detect physiological spatiotemporal pattern of synaptic inputs, such as sequential synaptic inputs (Ishikawa and Ikegaya, 2020). Therefore, a frame rate between 100 and 333 Hz is suitable for this protocol.

The dissociation constant (K_d) of the calcium indicators also determines the SN ratio. Lower K_d values are linked to greater power to detect calcium events but may mask the true calcium dynamics through higher calcium-buffering ability. On the other hand, higher K_d values lead to lower signal-detection power and result in lower SN ratios. Based on our experiences, appropriate K_d values for fMsCI range from 100 nM to 5 μM. We mainly used Fluo-4 (K_d = 345 nM) and Fluo-5F (K_d = 2.3 μM) (Figure 11).

The spatial resolution is also greatly improved and can distinguish the calcium activity of one spine from that of the neighboring spines; nevertheless, we sometimes encounter low SN ratios when we record activity in higher frame rates. Therefore, we also propose an offline denoising filter for calcium signals in spines. One of the most computationally efficient denoising methods is the Okada filter (Okada et al., 2016). However, the Okada filter replaces the fluorescence value (x_t) at the focused time, t, with the mean of the preceding and following values, $(x_{t-1} + x_{t+1})/2$, unless x_t is the median of three successive values, x_{t-1}, x_t, and x_{t+1}; therefore, the Okada filter inevitably blunts the peaks of individual calcium transients and prevents precise estimation of the signal magnitudes. Thus, we use a modified version of the Okada filter in which x_t is replaced with $(x_{t-1} + Zx_t + x_{t+1})/(2 + Z)$ unless x_t is the median. The coefficient Z represents the signal saliency against background noise and is defined as $(x_{t+1} - M)/SD$, where the mean M ($\bar{x}$) and the standard deviation SD (σ_x) are calculated from the entire time series $\{x_t\}$ (Figure 8); note that Z should refer to x_{t+1} instead of x_t to remove sharp shot noise without affecting the signal waveforms. As a result, the modified Okada filter smooths background noise without affecting the calcium transient peaks. The modified Okada filter can be applied repetitively to denoise calcium traces. Filtering twice results in the greatest improvement in the SN ratios of fMsCI datasets (Figure 9), and overfiltering may blunt the peaks of individual calcium transients.

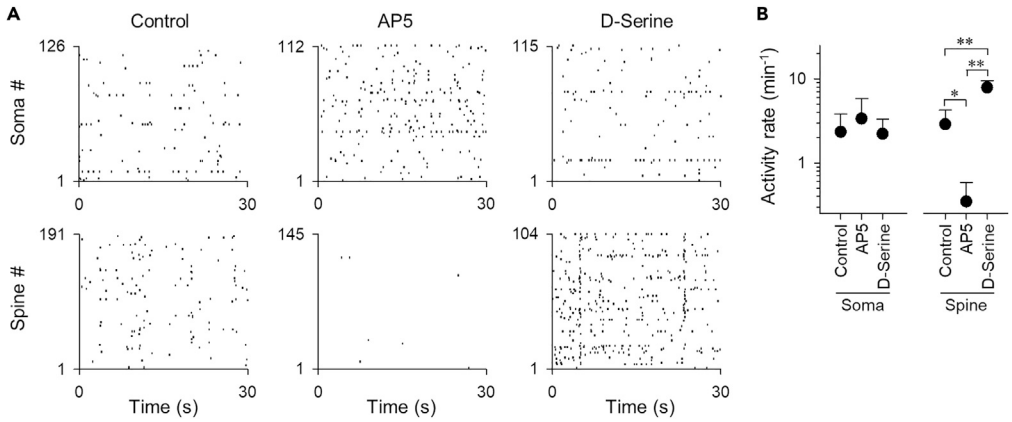

Figure 10. Effects of NMDA Receptor Modulation on Spine Calcium Activity Rates

(A) Representative raster plots of calcium activity recorded from multiple cell bodies (top) or from multiple spines (bottom) in the absence (control) or presence of 50 μM D-AP5 or 5 μM D-serine in the bath.

(B) Means ± SDs of calcium activity rates of 1,087, 582, and 505 cell bodies and 2,338, 640, and 531 spines from 4 to 10 slices among the three conditions. Only spine activity was significantly decreased and increased by D-AP5 and D-serine, respectively. Somatic activity rate: $P = 0.49$, $F_{2,17} = 0.74$, one-way ANOVA; spine activity: $P = 2.18 \times 10^{-6}$, $F_{2,15} = 35.2$, Scheffe's F test after one-way ANOVA. *$p < 0.05$; **$p < 0.01$.

fMsCI can be combined with whole-cell recordings from the cell bodies because the membrane potentials are voltage clamped using patch-clamp pipettes. The reversal potential can be modified by the intrapipette concentration of chloride ions; thus, either excitatory postsynaptic currents (EPSCs) or inhibitory postsynaptic currents (IPSCs) can be made dominant, depending on the purpose of the experiment (Figure 6). Such current isolation provides a unique opportunity to directly compare individual synaptic inputs to somatic excitation or inhibition (Kobayashi et al., 2019; Takahashi et al., 2016).

The spatiotemporal patterns of synaptic inputs affect neuronal spike outputs; however, the synaptic activity patterns under natural conditions have not been completely clarified. This protocol provides a unique opportunity for high-speed recordings of activity from hundreds of spines across multiple dendritic branches of a single neuron in combination with whole-cell electrophysiological recordings from the cell body. Because of its high SN ratio, our method does not require a trial averaging process and can reconstruct spine activity, including spontaneous activity, from single trials.

LIMITATIONS

Though other calcium indicators applicable for this method, Fluo-4 and Fluo-5F are more suitable for this method than other calcium indicators, such as Oregon Green BAPTA-1. In our experience using Oregon Green BAPTA-1, we were able to observe calcium activity from only a few spines and suffered from severe phototoxicity. As shown in Figure 11C, the S/N ratio of Fluo-4 was better than that of Fluo-5F (n = 100 spines each from 10 cells and 11 cells, respectively. $P = 8.25 \times 10^{-38}$, $t_{182} = 16.8$, Welch's t-test).

The fMsCI described here allows the imaging of calcium transients with high SN ratios in dendritic spines (Figure 4). The spatial resolution is also highly improved and can distinguish the calcium activity of one spine from the activity of the neighboring spines; nevertheless, we sometimes experience low SN ratios when we record activity in higher frame rates. Therefore, we use an offline filtering algorithm, the Okada filter (Okada et al., 2016), with a small modification. The original idea of the Okada filter employs a compromise strategy of the simple moving average filter and the median filter. Advantages of the Okada filter include computational speed and the preservation of signal waveforms. However, it reduces the peak amplitude of each calcium transient due to substitutions

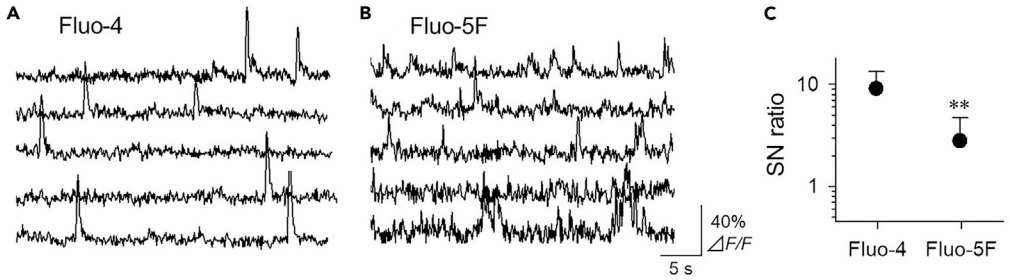

Figure 11. Effects of Calcium-Sensitive Fluorophores (Fluo-4 and Fluo-5F) on the SN Ratios of Spine Calcium Activity

(A and B) Five representative raw traces of calcium activity recorded from Fluo-4-loaded (A) and Fluo-5F-loaded spines at a frame rate of 10 Hz (B).

(C) Means ± SDs of the SN ratios in 100 spines. The SN ratio was defined as the mean calcium transient amplitude divided by the SD of the background noise. $P = 8.25 \times 10^{-38}$, $t_{182} = 16.8$, Welch's *t*-test.

of the peak values, x_t, with the neighboring mean, $(x_{t-1} + x_{t+1})/2$. To avoid this peak signal smoothing, we introduced the coefficient Z in the equation in Figure 8A. In the modified Okada filter, if x_t is not the median, x_t is substituted with $(x_{t-1} + Zx_t + x_{t+1})/(2 + Z)$. This process is repeated serially from the second frame to the penultimate frame, whereas the values from the first frame and the last frame are not changed. For calcium traces recorded at 100 Hz, the SN ratio was the highest when the modified Okada filter was applied twice (Figure 9).

TROUBLESHOOTING

Problem 1

Poor visibility of dendritic branches (step 12).

Potential Solution 1

Work with another cell or slice if cells or tissues are unhealthy. Cell and tissue health affect the quality of dye loading.

Try to decrease the series resistance or patch another neuron when series resistance is high. Wait for a long enough period of time to load the dye with the neuron and spines.

Problem 2

Poor visibility of spine activity (step 14).

Potential Solution 2

Try to decrease the series resistance and wait for a longer period of time for the somatic whole-cell recording.

Reduce the laser power and exposure time as much as possible to avoid photodamage.

Problem 3

Dendritic blebbing (step 14).

Potential Solution 3

Reduce the laser power and exposure time as much as possible to avoid photodamage.

Problem 4

Leak current increasing (step 14).

Potential Solution 4

Change the preparation or improve the quality of patch-clamping.

Reduce the laser power and exposure time as much as possible.

Problem 5

Large motion artifacts (step 16).

Potential Solution 5

Adjust the position and speed of aCSF perfusion.

Put the platinum ring on a wider range of the membrane.

RESOURCE AVAILABILITY

Lead Contact

Further information and requests for resources and reagents should be directed to and will be fulfilled by the Lead Contact, Tomoe Ishikawa (tomoe.y.ishikawa@gmail.com).

Materials Availability

This study did not generate new unique materials. All materials are purchasable.

Data and Code Availability

All data needed to evaluate the conclusions in the paper are present in the paper. Additional data and codes related to this paper may be requested from the authors.

ACKNOWLEDGMENTS

This work was supported by JST ERATO (JPMJER1801), JSPS Grants-in-Aid for Scientific Research (18H05525 and 17H07086), a Sasakawa Scientific Research Grant from the Japan Science Society (2018-4008), and the Human Frontier Science Program (RGP0019/2016). This work was conducted partially as a program at the International Research Center for Neurointelligence (WPI-IRCN) of The University of Tokyo Institutes for Advanced Study at The University of Tokyo.

AUTHOR CONTRIBUTIONS

Conceptualization, T.I., C.K., N.T., and Y.I.; Data acquisition T.I., C.K., and N.T.; Data analysis, T.I, and Y.I.; Writing – Original Draft, T.I. and Y.I.; Writing – Review & Editing, T.I., C.K., N.T., and Y.I.

DECLARATION OF INTERESTS

The authors declare no competing interests.

REFERENCES

Bischofberger, J., Engel, D., Li, L., Geiger, J.R., and Jonas, P. (2006). Patch-clamp recording from mossy fiber terminals in hippocampal slices. Nat. Protoc. *1*, 2075–2081.

Branco, T., Clark, B.A., and Häusser, M. (2010). Dendritic discrimination of temporal input sequences in cortical neurons. Science *329*, 1671–1675.

Chen, X., Leischner, U., Varga, Z., Jia, H., Deca, D., Rochefort, N.L., and Konnerth, A. (2012). LOTOS-based two-photon calcium imaging of dendritic spines in vivo. Nat. Protoc. *7*, 1818–1829.

De Simoni, A., and Yu, L.M. (2006). Preparation of organotypic hippocampal slice cultures: interface method. Nat. Protoc. *1*, 1439–1445.

Guthrie, P.B., Segal, M., and Kater, S.B. (1991). Independent regulation of calcium revealed by imaging dendritic spines. Nature *354*, 76–80.

Ishikawa, T., and Ikegaya, Y. (2020). Locally sequential synaptic reactivation during hippocampal ripples. Sci. Adv. *6*, eaay1492.

Kobayashi, C., Okamoto, K., Mochizuki, Y., Urakubo, H., Funayama, K., Ishikawa, T., Kashima, T., Ouchi, A., Szymanska, A.F., Ishii, S., et al. (2019). GABAergic inhibition reduces the impact of synaptic excitation on somatic excitation. Neurosci. Res. *146*, 22–35.

Koyama, R., Muramatsu, R., Sasaki, T., Kimura, R., Ueyama, C., Tamura, M., Tamura, N., Ichikawa, J., Takahashi, N., Usami, A., et al. (2007). A low-cost method for brain slice cultures. J. Pharmacol. Sci. *104*, 191–194.

Long, F., Zeng, S., and Huang, Z.L. (2012). Localization-based super-resolution microscopy with an sCMOS camera part II: experimental methodology for comparing sCMOS with EMCCD cameras. Opt. Express *20*, 17741–17759.

Losonczy, A., Makara, J.K., and Magee, J.C. (2008). Compartmentalized dendritic plasticity and input feature storage in neurons. Nature *452*, 436–441.

Müller, W., and Connor, J.A. (1991). Dendritic spines as individual neuronal compartments for synaptic Ca2+ responses. Nature *354*, 73–76.

Okada, M., Ishikawa, T., and Ikegaya, Y. (2016). A Computationally Efficient Filter for Reducing Shot Noise in Low S/N Data. PLoS One *11*, e0157595.

Okamoto, K., Ishikawa, T., Abe, R., Ishikawa, D., Kobayashi, C., Mizunuma, M., Norimoto, H., Matsuki, N., and Ikegaya, Y. (2014). Ex vivo cultured neuronal networks emit in vivo-like spontaneous activity. J. Physiol. Sci. *64*, 421–431.

Poirazi, P., Brannon, T., and Mel, B.W. (2003). Pyramidal neuron as two-layer neural network. Neuron *37*, 989–999.

Sakaguchi, T., Okada, M., and Kawasaki, K. (1994). Sprouting of CA3 pyramidal neurons to the dentate gyrus in rat hippocampal organotypic cultures. Neurosci. Res. *20*, 157–164.

Sasaki, T., Takahashi, N., Matsuki, N., and Ikegaya, Y. (2008). Fast and accurate detection of action potentials from somatic calcium fluctuations. J. Neurophysiol. *100*, 1668–1676.

Schindelin, J., Arganda-Carreras, I., Frise, E., Kaynig, V., Longair, M., Pietzsch, T., Preibisch, S., Rueden, C., Saalfeld, S., Schmid, B., et al. (2012). Fiji: an open-source platform for biological-image analysis. Nat. Methods *9*, 676–682.

Takahashi, N., Sasaki, T., Matsumoto, W., Matsuki, N., and Ikegaya, Y. (2010). Circuit topology for synchronizing neurons in spontaneously active networks. Proc. Natl. Acad. Sci. U S A *107*, 10244–10249.

Takahashi, N., Oba, S., Yukinawa, N., Ujita, S., Mizunuma, M., Matsuki, N., Ishii, S., and Ikegaya, Y. (2011). High-speed multineuron calcium imaging using Nipkow-type confocal microscopy. Curr. Protoc. Neurosci., Chapter 2, Unit 2.14.

Takahashi, N., Kitamura, K., Matsuo, N., Mayford, M., Kano, M., Matsuki, N., and Ikegaya, Y. (2012). Locally synchronized synaptic inputs. Science *335*, 353–356.

Takahashi, N., Kobayashi, C., Ishikawa, T., and Ikegaya, Y. (2016). Subcellular imbalances in synaptic activity. Cell Rep. *14*, 1348–1354.

Varga, Z., Jia, H., Sakmann, B., and Konnerth, A. (2011). Dendritic coding of multiple sensory inputs in single cortical neurons in vivo. Proc. Natl. Acad. Sci. U S A *108*, 15420–15425.

Yuste, R., and Denk, W. (1995). Dendritic spines as basic functional units of neuronal integration. Nature *375*, 682–684.